Error bounds on ultrasonic scatterer size estimates

Pawan Chaturvedi and Michael F. Insana
Department of Radiology, University of Kansas Medical Center, Kansas City, Kansas 66160-7234

(Received 20 November 1995; accepted for publication 17 January 1996)

Precision errors that occur in estimating the average scatterer size from pulse-echo ultrasound waveforms are examined in detail. The method-independent lower bound on estimation error is found from the Cramér–Rao inequality for comparison with the predicted error for the measurement technique currently used to estimate scatterer sizes in soft biological tissues. The probability density function for the estimate is also derived. From these statistical analyses, strategies for designing experiments that minimize the error are discussed. It is shown that compared with biological variability, measurement errors in scatterer size estimates are relatively large. Consequently, there is reason to continue searching for more efficient estimators. Although the analysis and results are derived for Gaussian correlation models that have been used to study the function and structure of kidneys, generalization to include correlation models for other tissues is straightforward. © *1996 Acoustical Society of America.*

PACS numbers: 43.60.Pt, 43.80.Cs, 43.80.Ev [JLK]

INTRODUCTION

Characterization of soft tissue microstructure is a principal goal of quantitative ultrasonic analysis. Specifically, the average scatterer size D has been found to be particularly sensitive to renal microvascular changes that occur early in disease processes but cannot be measured by other means.[1,2] For D to become an important new diagnostic indicator, it must be possible to reliably detect variations in vascular lumen as small as 20%.[1–3] Although luminal changes can be as large as 90%,[2] the range of variations that can be detected in any one scatterer size image is determined by the dynamic range of the measurement. Accurate detection of small changes is limited by precision errors introduced at various steps of the estimation process. In order to assess the clinical potential of scatterer size estimates and the performance of any particular estimation technique, it is essential to understand the nature of errors in the measurement process.

The purpose of the following analyses is threefold. First, we derive the method-independent lower bound on the mean-square error (MSE) ϵ_D^2 based on the Cramér–Rao inequality. This bound establishes the lowest possible error for estimating scatterer sizes and is independent of the estimation method. Second, we derive expressions that predict the variance of the estimate var $\hat{D}$ as a function of the analysis bandwidth for the maximum likelihood technique we currently use to study kidneys. Comparisons of ϵ_D^2 and var $\hat{D}$ yield the efficiency of the estimator for renal analysis. Third, we derive the probability density function (pdf) of the scatterer size parameter D at a particular spatial frequency k: $p(D;k)$. The results are verified through echo signal simulations. Together these three analyses may be used to optimize the experimental design and explain the empirical findings reported earlier.

I. SCATTERING MODEL AND ESTIMATION TECHNIQUE

A standard single-scatter model[4,5] is often used to interpret acoustic backscatter measurements from soft biological media in terms of the underlying random structure.[6–8] The backscatter coefficient[9–11] is the quantity that links mathematical models of acoustic scattering with ultrasonic measurements, and is the basis for scatterer size estimates in the eye,[8] heart,[12] and kidney.[13] Due to their extensive use in the analyses that follow, in this section we summarize the analysis techniques that have been described previously.[7,10,11]

For plane-wave incidence and far-field observation of a weakly scattering, continuous, isotropic, random medium, the backscatter coefficient $\sigma_b(k)$ is (Section D of Ref. 15)

$$\sigma_b(k)=\sigma_0 F(k,D), \tag{1a}$$

where

$$\sigma_0=k^4 V_s E\{\gamma^2\}/16\pi^2, \tag{1b}$$

$$F(k,D)=\frac{2\pi}{kV_s}\int_0^\infty b_\gamma(\Delta r)\sin(2k\Delta r)\,d\Delta r. \tag{1c}$$

The relationship between spatial frequency k, temporal frequency f, wavelength λ, and sound speed c is $k=2\pi/\lambda=2\pi f/c$. The backscatter coefficient in Eq. (1a) has been factored into the product of the Rayleigh scattering coefficient σ_0 and the form factor $F(k,D)$. By studying the form factor, we can isolate important structural features of tissue morphology and function, such as scatterer size and shape, independent of other features, such as scatterer number density, impedance, attenuation, and measurement system response.

The ''scattering structure'' of a tissue is $\gamma(r)$, a function that defines the fluctuations in the microscopic elastic properties of a medium. The structure of a continuous, stationary, random scattering medium is summarized by the autocorrelation function $E\{\gamma(r_1)\gamma(r_2)\}=E\{\gamma^2(r)\}b_\gamma(\Delta r)$, where $E\{\cdots\}$ indicates the expected value of the argument and $b_\gamma(\Delta r)$ is the correlation coefficient (also referred to as the normalized autocorrelation function in some signal processing literature) (Appendix B of Ref. 15). The correlation coefficient for this stationary random process is a function of relative position in the medium $\Delta r=r_1-r_2$. Using this

 0001-4966/96/100(1)/392/8/$6.00

model, it can be shown[15] that for far-field observation, the form factor of Eq. (1c) is the Fourier transform of the correlation coefficient normalized by the effective volume of the scattering site, $V_s \equiv \int_{-\infty}^{\infty} b_\gamma(\Delta r) dv_\Delta$.

The effective scatterer size D in random continua is defined relative to the characteristic dimension of the correlation function d by equating the spherical volume $4\pi(D/2)^3/3$ with V_s as calculated for a specific correlation model function. For example, the spherically symmetric Gaussian correlation model of correlation length d,

$$b_\gamma(\Delta r) = \exp(-\Delta r^2/2d^2), \tag{2a}$$

yields[15]

$$D/d = (12\sqrt{2\pi})^{1/3} \simeq 3.11 \equiv d_1. \tag{2b}$$

Consequently, Eq. (1a) provides the requisite relationship between backscatter measurements and tissue microstructure needed to estimate an average scatterer size.

Our estimation strategy is to first identify a correlation model function b_γ that is representative of the test sample under investigation. We have shown previously[1,13] that a multicomponent version of the Gaussian model in Eq. (2a) is well suited to the investigation of microvascular anatomy and function in the renal cortex. For the chosen b_γ, a set of form factor model functions $F(k,D)$ is computed for the measurement bandwidth of (spatial) frequencies $k_1 \leqslant k \leqslant k_2$ and scatterer sizes $D_1 \leqslant D \leqslant D_2$ possible in the sample. A small amount of prior information, obtained through histological analysis, is used to find these limits. Subsequently, backscatter coefficients are measured[7,10] for the test sample and the corresponding form factors are estimated.[14] Finally, we determine the estimate $\hat{D}$ from the model function F that produces the smallest mean square difference when compared to the measurement $\hat{F}$.

How efficient is this strategy? That is, how well does this estimator use the available information to perform its task? The results of the next two sections provide a partial answer.

II. THE CRAMÉR–RAO LOWER BOUND (CRLB)

In this section, the lower bound on the MSE for scatterer size estimation, ϵ_D^2, is derived from the Cramér–Rao inequality. For this purpose, it is convenient to consider a discrete sampling[16] of the continuous echo waveform. Assume $\hat{D}$ to be an unbiased estimate of scatterer size, i.e., $E\{\hat{D}\} - D = 0$, as determined from an analysis of the measurement vector $\mathbf{x}^t = (x[0], x[1], \ldots, x[N-1])$. $\mathbf{x}^t$ is the transpose of the N-point column vector $\mathbf{x}$. We further assume that the likelihood function $p(\mathbf{x};D)$, which represents a family of pdf's comprised of one density function for each deterministic D value, is known. From the likelihood function, we find the variance of the estimate:

$$\begin{aligned} \operatorname{var} \hat{D} &= E\{(\hat{D} - D)^2\} \\ &= \int_{-\infty}^{\infty} (\hat{D} - D)^2 p(\mathbf{x};D) d\mathbf{x} \quad \text{for all } D. \end{aligned}$$

Consequently, $\operatorname{var} \hat{D}$ is a function of D. It is well known[17] that if $\partial p/\partial D$ exists, then $\operatorname{var} \hat{D}$ can be no smaller than ϵ_D^2, i.e.,

$$\operatorname{var} \hat{D} \geqslant \epsilon_D^2 = \left[-E\left\{ \frac{\partial^2 \ln p(\mathbf{x};D)}{\partial D^2} \right\} \right]^{-1}, \tag{3}$$

where the result after taking derivatives is evaluated at a specific value for D. Equation (3) is the Cramér–Rao inequality, and ϵ_D^2 is the CRLB on the estimation error. We now describe a linear model of echo-signal formation that enables us to solve Eq. (3) by constructing a likelihood function that is both consistent with experimental observations[18] and mathematically tractable.[19]

The measurement vector $\mathbf{x}$ is modeled as the sum of the echo signal $\mathbf{s}$ and measurement noise $\mathbf{n}$. For the ith temporal sample,

$$x[i] = s[i] + n[i] \quad 0 \leqslant i \leqslant N-1, \tag{4}$$

where all terms are random variables. Noise samples are drawn from a zero-mean Gaussian white process, as indicated by the notation $\mathcal{N}(0,\sigma_n^2)$, and are assumed to be uncorrelated with each other and with the signal samples. The echo signal is $s[i] = g[i] * \gamma_{\langle m \rangle}[i]$, the convolution of a spatially invariant[20] pulse-echo impulse response of the measurement system g with the reflectivity profile of the medium γ. The pulse-echo impulse response is the convolution of the transmitted and received impulse responses: $g[i] = g_{\text{tran}}[i] * g_{\text{rec}}[i]$. Furthermore, the reflectivity profile is another linear process, $\gamma_{\langle m \rangle}[i] = t[i] * r_{\langle m \rangle}$, where $r_{\langle m \rangle} = \mathcal{N}(0,\sigma_r^2)$ and $t[i]$ is the tissue impulse response, such that $b_\gamma[i-j] = E\{t[i]t[j]\}/E\{t^2[i]\}$. To summarize the details of Eq. (4),

$$x[i] = \underbrace{g[i] * t[i]}_{h[i]} * r_{\langle m \rangle} + n[i] = h[i] * r_{\langle m \rangle} + n[i],$$

$$0 \leqslant i \leqslant N-1, \tag{5}$$

where $h[i]$ is a spatially invariant filter that combines properties of the pulse and tissue[19] such that when it is convolved with the spatially variant random process $r_{\langle m \rangle}$ and added to measurement noise $n[i]$, we generate a measurement sample with the essential properties of an ultrasonic echo signal $x[i]$.

Based on this model, the likelihood function is multivariate Gaussian $\mathcal{N}(\mathbf{0},\mathbf{K}(D))$. More specifically,

$$\begin{aligned} p(\mathbf{x};D) &= \prod_i p(x_i;D) \\ &= [(2\pi)^N \det \mathbf{K}]^{-1/2} \exp(-\tfrac{1}{2}\mathbf{x}^t\mathbf{K}^{-1}\mathbf{x}), \end{aligned} \tag{6}$$

where $\mathbf{K} = E\{\mathbf{x}\mathbf{x}^t\} = E\{\mathbf{s}\mathbf{s}^t\} + \sigma_n^2\mathbf{I}$ is the covariance matrix of the data $\mathbf{x}$, $\mathbf{I}$ is the identity matrix, $\det \mathbf{K}$ is the determinant of $\mathbf{K}$ and $\mathbf{K}^{-1}$ is its inverse. Notice that $\mathbf{x}$ and $\mathbf{K}$ are functions of D.

Let the total correlation time be L points for the incident ultrasonic pulse and M points for the tissue impulse response. The total correlation time is defined as the maximum lag $j-i$ of the autocorrelation function $E\{h[i]h[i+(j-i)]\}$ for which the autocorrelation function is essentially

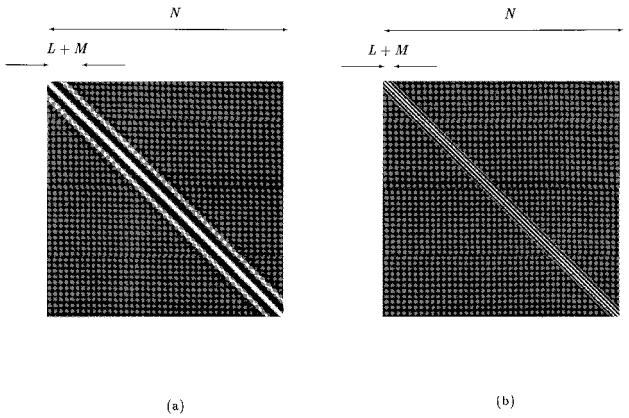

FIG. 1. Images of the covariance matrix for $N=256$ and SNR=40 dB. (a) D/FWHM~1 and (b) D/FWHM~0.02.

nonzero.[17] For typical situations, the echo signal has a large time-bandwidth product ($L+M \ll N$) and elements of the covariance matrix are given by

$$K_{i,j}=\begin{cases} E\{s^2[i]\}+\sigma_n^2=\sigma_r^2\Sigma_i(h[i])^2+\sigma_n^2, & i=j, \\ E\{s[i]s[j]\}=\sigma_r^2\Sigma_i h[i]h[i-(i-j)], & \\ \qquad\qquad 0<|i-j|<L+M, & \\ 0, \qquad\qquad L+M\geqslant|i-j|\geqslant N\ . & \end{cases} \tag{7}$$

Using the notation $H(k)=\mathscr{F}\{h[l]\}=\Sigma_{l=0}^{\infty}h[l]\times\exp(-ilkc\Delta t)$ and $h[l]=\mathscr{F}^{-1}\{H(k)\}$ to indicate discrete-time Fourier transform pairs, we express the covariance matrix elements of Eq. (7) as

$$\begin{aligned} E\{s[i]s[j]\}&=\sigma_r^2\mathscr{F}^{-1}\{|H(k)|^2\} \quad 0\leqslant|i-j|<L+M \\ &=\sigma_r^2\mathscr{F}^{-1}\{|T(k)|^2|G(k)|^2\}, \end{aligned} \tag{8a}$$

where $|H(k)|^2$ is the squared modulus of the complex transform $H(k)$,

$$|T(k)|^2=k^4F(k,D)=k^4\ \exp(-2k^2D^2/d_1^2) \tag{8b}$$

and

$$\begin{aligned} |G(k)|^2=\tfrac{1}{4}[&\exp(-(k+k_0)^2\sigma_g^2)-2\exp(-(k^2+k_0^2)\sigma_g^2) \\ &+\exp(-(k-k_0)^2\sigma_g^2)]. \end{aligned} \tag{8c}$$

The right-hand side of Eq. (8b) was found by combining Eqs. (1c)–(2b), and Eq. (8c) is the power spectral density of a pulse function $g[i]$ modeled as a sine wave of frequency k_0 with a Gaussian-modulated envelope of characteristic dimension σ_g. Note that $|T(k)|^2$ is a function of the form factor.

The covariance matrix of Eq. (8a) is Toeplitz as illustrated in Fig. 1. In Fig. 1(a), the scatterer size D has been selected to be equal to the full-width-at-half-maximum (FWHM) ultrasonic pulse length of 1 mm.[21] In Fig. 1(b), however, D has been reduced to 25 μm while the pulse length is unchanged. As the scatterer size increases from a point ($L\gg M$) to the size of the pulse ($L\simeq M$), the correlation length of the $h[i]$ filter increases.

We now have all the parts necessary to construct a likelihood function. From Eq. (6),

$$\ln\ p(\mathbf{x};D)=-\tfrac{1}{2}(\ln[(2\pi)^N\ \det\ \mathbf{K}]+\mathbf{x}^t\mathbf{K}^{-1}\mathbf{x}). \tag{9}$$

The partial differentiation of Eq. (3) was computed using the difference approximation:[19]

$$\left(\frac{\partial^2\ \ln\ p}{\partial D^2}\right)_D\simeq\frac{\ln\ p|_{D-\Delta D}-2\ \ln\ p|_D+\ln\ p|_{D+\Delta D}}{\Delta D^2}, \tag{10}$$

where ΔD is an incremental change about a specific value of D.

Two sets of echo data were simulated to investigate the behavior of the CRLB developed in this section. With the first set, we explored the relationship between ϵ_D and the input signal-to-noise ratio (SNR). With the second set, we explored the relationship between ϵ_D and D, and examined an asymptotic CRLB expression. SNR was defined as the ratio of signal power to noise power at center frequency k_0,

$$\mathrm{SNR(dB)}=10\log\left(\frac{|S(k_0)|^2}{|N(k_0)|^2}\right). \tag{11}$$

A more commonly used definition of the SNR for the data model given by Eq. (7) is

$$\mathrm{SNR(dB)}=10\log\left(\frac{\sigma_r^2\Sigma_i(h[i])^2}{\sigma_n^2}\right). \tag{12}$$

When the spectral shape is the same for both signal and noise, the two definitions are equivalent. When the signal spectrum is Gaussian and the noise is white, as in the experiments presented in this paper, Eq. (11) is more conservative and results in an SNR level that is higher by approximately 3.9 dB compared to the definition given in Eq. (12).

Echo signals were simulated with a center frequency of 5 MHz [$k_0=2\pi\times5$ MHz/(1.54 mm/μs)=20.4 mm^{-1}], a sampling rate of 2.5×10^7 samples per second, and $N=256$ points per waveform. The partial derivatives of the log-likelihood function were evaluated using Eq. (10) with $\Delta D=2.0$ μm, and the expectation was approximated by averaging the results from 100 realizations of $\mathbf{x}$. The covariance matrix was computed using Eqs. (7) and (8), where we set $\sigma_r^2=1$, $\sigma_g^2=0.03$ mm^2, and σ_n^2 was found from Eq. (12). Finally, ϵ_D was estimated using Eq. (3).

In the first study, D was fixed at 100 μm. As shown in Fig. 2, ϵ_D decreases rapidly as the SNR increases from 0 to 40 dB.

In the second study, we sought to validate our ϵ_D results by comparisons with those of an asymptotic CRLB expression (Section 3.10 of Ref. 17). For zero-mean echo signals having bandlimited power spectral density (PSD) $P_{xx}(k)$, the asymptotic CRLB for D, $\tilde{\epsilon}_D^2$, is given by

$$\tilde{\epsilon}_D^{\,2}=\left[\frac{N}{2}\int_{-1/2}^{1/2}\left(\frac{\partial\ \ln\ P_{xx}(k;D)}{\partial D}\right)^2dk\right]^{-1}\overset{N\gg L+M}{\longrightarrow}\epsilon_D^2. \tag{13}$$

The advantage of using Eq. (13) is its ease of calculation. When the time-bandwidth product is large, $\tilde{\epsilon}_D$ is approximately equal to ϵ_D. [In our simulations, $N/(L+M)>10$. For example, see Fig. 1.] To compute Eq. (13), P_{xx} may be obtained from the scattering model of Eq. (8):

$$P_{xx}(k)=c_1k^4F(k)|G(k)|^2, \tag{14}$$

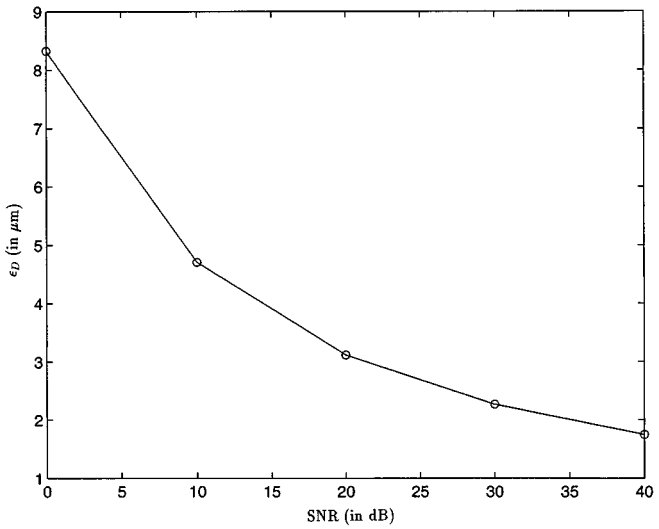

FIG. 2. Variation of the CRLB with the input SNR.

where c_1 is a frequency-independent constant. Values of $\tilde{\epsilon}_D$ that result from Eqs. (13) and (14) are shown in Fig. 3 along with the ϵ_D results. Both curves are plotted as a function of D from 65 through 110 μm and for SNR=40 dB. The two curves, which are very similar, show that errors decrease for larger scatterer sizes in this range, and that the lower bound on the MSE is small compared to the mean value.

III. VARIANCE OF THE SCATTERER DIAMETER ESTIMATES

Realistic estimates of var $\hat{D}$ must account for all sources of measurement error, including those introduced by the method of data reduction. The quantity ϵ_D^2, derived in the previous section, is independent of the estimation technique; it depends only on the total information contained in **x**. While the CRLB may not be achievable in practice, it established the ''best possible'' performance for scatterer size estimation. In this section, we develop an analytical expression for var $\hat{D}$ that may be achieved experimentally using the estimation procedures described in Sec. I.

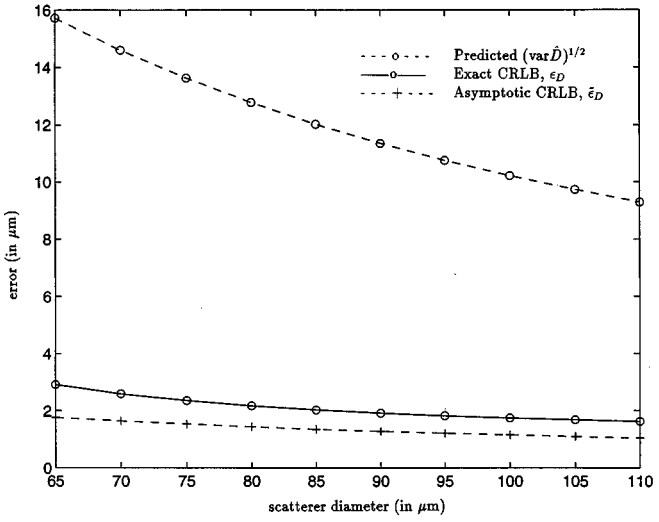

FIG. 3. Exact [Eq. (3)] and asymptotic [Eq. (13)] expressions for the CRLB on $\hat{D}$ error are plotted with the predicted standard deviation of the estimate [Eq. (26)] as a function of scatterer size.

As previously described, scatterer sizes are measured from the form factor, which is determined from $\hat{P}_{xx}$, the estimated PSD, of the data. The popular periodogram PSD estimator[22] for the data of Eq. (5) is

$$\hat{P}_{xx}(k)=\frac{\Delta t}{N}\left|\sum_{l=1}^{N-1} x[l]\exp(-ilkc\Delta t)\right|^2=\frac{1}{N\Delta t}\,|X(k)|^2, \tag{15}$$

where Δt is the sampling interval and $X(k)=\mathcal{F}\{x\}$. For a periodogram, the variance of each estimate in the analysis bandwidth is given by (Appendix 4.A of Ref. 22):

$$\text{var}\ \hat{P}_{xx}(k)\approx[P_{xx}(k)]^2 q(k), \tag{16}$$

where $P_{xx}(k)$ is the expected or ''true'' PSD, and

$$q(k)=\left[1+\left(\frac{\sin(kcN\Delta t)}{N\sin(kc\Delta t)}\right)^2\right]. \tag{17}$$

From the definition in Eq. (15), a periodogram is seen to be an inconsistent estimator since the variance of an estimate does not approach zero as the length of the signal N is increased to infinity. Rather, var $\hat{P}_{xx}(k) \overset{N\to\infty}{\rightarrow} [P_{xx}(k)]^2$.

Our goal is to obtain var $\hat{D}$ from knowledge of var $\hat{P}_{xx}$ as given by Eq. (16). Fixing the scatterer size, we write $F(k)\equiv F(k,D)|_D$, and combining Eqs. (14) and (16) gives

$$\text{var}\ \hat{F}(k)=[c_1 k^4|G(k)|^2]^{-2}\ \text{var}\ \hat{P}_{xx}(k)\approx[F(k)]^2 q(k). \tag{18}$$

The estimate $\hat{D}$ is obtained by determining the minimum mean-square difference between the form factor for the true scatterer size, given by Eq. (8b), and the measurement $\hat{F}$. Therefore, the problem of measuring $\hat{D}$ is essentially one of minimizing χ^2 as defined by

$$\chi^2=\sum_{i=1}^{K}\frac{1}{\text{var}\ \hat{F}(k_i)}\{\hat{F}(k_i)-\exp(-2k_i^2D^2/d_1^2)\}^2, \tag{19}$$

where K is the number of points included in the analysis bandwidth over which $\hat{F}$ and F are compared. A compact mathematical expression of our scatterer size estimator is

$$\hat{D}=\arg\min_D \chi^2. \tag{20}$$

To solve Eq. (20), we take the derivative of Eq. (19) with respect to D and set it equal to zero:

$$\sum_{i=1}^{K}\frac{k_i^2}{\text{var}\ \hat{F}(k_i)}\exp\left\{-\frac{2k_i^2D^2}{d_1^2}\right\}\times\left[\hat{F}(k_i)-\exp\left\{-\frac{2k_i^2D^2}{d_1^2}\right\}\right]=0. \tag{21}$$

The estimate $\hat{D}$ is the value of D that satisfies Eq. (21). The variance of this estimate can be obtained by error propagation through the use of a Taylor series expansion.[23] Assuming that errors in $\hat{F}$ are not too large, so that we may ignore second- and higher-order partial derivatives, and that N is

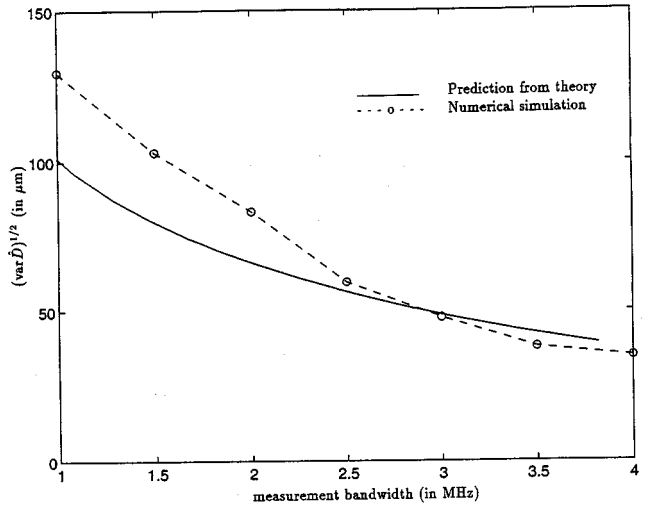

(a)

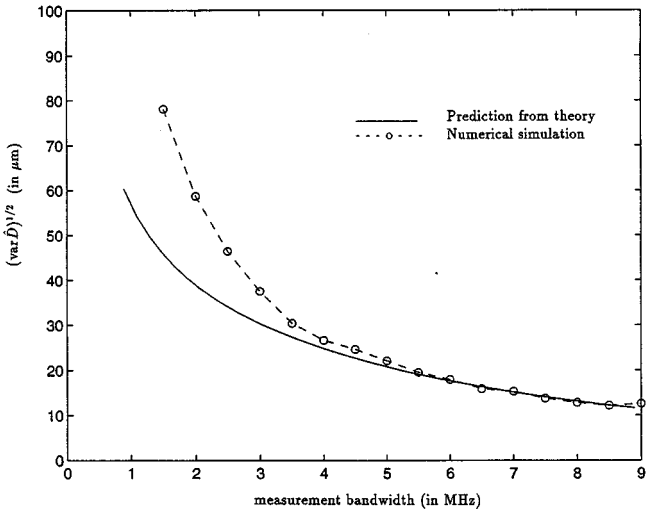

FIG. 4. Plot of the estimation error as a function of the measurement bandwidth. (a) Center frequency=3 MHz, $D=150$ μm and (b) center frequency=5 MHz, $D=100$ μm.

large, so that the $\hat{F}(k_i)$ are uncorrelated, var $\hat{D}$ may be expressed as

$$\text{var}\,\hat{D}\approx\sum_{j=1}^{K}\left\{\text{var}\,\hat{F}(k_j)\left(\frac{\partial D}{\partial\hat{F}(k_j)}\right)^2\right\}. \tag{22}$$

The small-error assumption is satisfied when $k_0a\equiv k_0D/2\sim 1$. If the average scatterer size for a medium is D, selecting a center frequency k_0 that satisfies this condition ensures that the form factor is sensitive to small changes in scatterer size,[14] and spectral noise is less detrimental to the estimate. This concept is discussed further in later sections.

To evaluate Eq. (22), an expression for the derivative of D with respect to $\hat{F}$ is required. The desired expression is obtained by differentiating Eq. (21) with respect to $\hat{F}(k_j)$. Let Y_i represent the summation arguments, so that Eq. (21) reads $\Sigma_{i=1}^{K}Y_i=0$. Using the chain rule,

$$\frac{\partial Y_i}{\partial\hat{F}(k_j)}=\frac{\partial Y_i}{\partial D}\,\frac{\partial D}{\partial\hat{F}(k_j)}, \tag{23}$$

it is straightforward to show from Eq. (21) that

$$\begin{aligned}\frac{\partial D}{\partial\hat{F}(k_j)}=&\left\{\frac{k_j^2d_1^2}{4D\ \text{var}\,\hat{F}(k_j)}\exp\left(-\frac{2k_j^2D^2}{d_1^2}\right)+v_j'\right\}\\&\times\left\{\sum_{i=1}^{K}\left[\frac{k_i^4}{\text{var}\,\hat{F}(k_i)}\exp\left(-\frac{2k_i^2D^2}{d_1^2}\right)\right.\right.\\&\left.\left.\times\left\{\hat{F}(k_i)-2\exp\left(-\frac{2k_i^2D^2}{d_1^2}\right)\right\}\right]\right\}^{-1},\end{aligned} \tag{24}$$

where v_j' represents the contribution from the derivative of var $\hat{F}(k_i)$. From Eq. (18),

$$\begin{aligned}v_j'\approx&-\sum_{i=1}^{K}k_i^2\exp\left(-\frac{2k_i^2D^2}{d_1^2}\right)\left[\frac{2F(k_i)}{(\text{var}\,\hat{F}(k_i))^2}\right.\\&\left.\times\left\{\hat{F}(k_i)-\exp\left(-\frac{2k_i^2D^2}{d_1^2}\right)\right\}\right]\frac{\partial F(k_i)}{\partial\hat{F}(k_j)},\end{aligned} \tag{25}$$

when N is large such that $q(k)\approx 1$. Substituting Eqs. (24) and (25) into Eq. (22) and simplifying, we find the following expression for the variance of $\hat{D}$:

$$\begin{aligned}\text{var}\,\hat{D}\approx&\frac{d_1^4}{16D^2}\left\{\sum_{i=1}^{K}\left[\frac{k_i^4}{\text{var}\,\hat{F}(k_i)}\exp\left(-\frac{2k_i^2D^2}{d_1^2}\right)\left\{\hat{F}(k_i)\right.\right.\right.\\&\left.\left.\left.-2\exp\left(-\frac{2k_i^2D^2}{d_1^2}\right)\right\}\right]\right\}^{-2}\sum_{j=1}^{K}\left\{\text{var}\,\hat{F}(k_j)\right.\\&\left.\times\left[v_j'+\frac{k_j^2}{\text{var}\,\hat{F}(k_j)}\exp\left(-\frac{2k_j^2D^2}{d_1^2}\right)\right]^2\right\}.\end{aligned} \tag{26}$$

Although Eq. (26) provides a closed-form expression for the variance, it cannot be evaluated analytically. Not only do we need expressions for the measurements and their variances, but we also need the derivatives of the measurements with respect to the model F to compute v_j'. Also, the complexity of the expression obscures much of the physical insight into Eq. (26). Expanding $\hat{F}$ in a Taylor series

$$\hat{F}=F+(\hat{F}-F)\,\frac{\partial F}{\partial\hat{F}}+\cdots$$

and preserving only the zeroth-order term such that $\hat{F}(k_i)\approx\exp(-2k_i^2D^2/d_1^2)$, we simplify the expression significantly. Combining Eqs. (18) and (26) gives

$$\text{var}\,\hat{D}\approx\frac{d_1^4}{16D^2}\left\{\sum_{i=1}^{K}\left[\frac{k_i^4}{q(k_i)}\right]\right\}^{-1}. \tag{27}$$

Equation (27) shows that var $\hat{D}$ is lower for large scatterers interrogated at high frequencies, provided $k_0a\approx 1$. The results of Eq. (27) are compared with those of the CRLB in Fig. 3.

Truncation of the Taylor series is expected to reduce the accuracy of Eq. (27). To appreciate how much, we examined two sets of simulated echo signals, at 3 and 5 MHz center frequencies, that were generated as described in Sec. II. Each

set consisted of four hundred independent waveforms. The simulated waveforms did not include additive noise in order to observe how var $\hat{D}$ varies with analysis bandwidth.

Using Fig. 4(a) and (b), we compared the results of Eq. (27) with those obtained from the simulated data. In Fig. 4(a), $D=150$ μm and $f_0=3$ MHz, and in Fig. 4(b), $D=100$ μm and $f_0=5$ MHz. Consequently, $k_0a\approx 1$ such that the form factor is most sensitive to changes in D. Only one echo waveform, 10.2 μs in duration ($N=256$ pts), was used to determine each $\hat{D}$ estimate. Bias errors for the simulated data were negligible. We observed that the errors predicted by Eq. (27) are very similar to the measured errors involving echo simulations when the analysis bandwidth exceeds 80% of the center frequency. For smaller bandwidths, higher-order terms in the Taylor series applied to Eq. (26) cannot be ignored and there is less agreement between the simulations and the prediction from the theory.

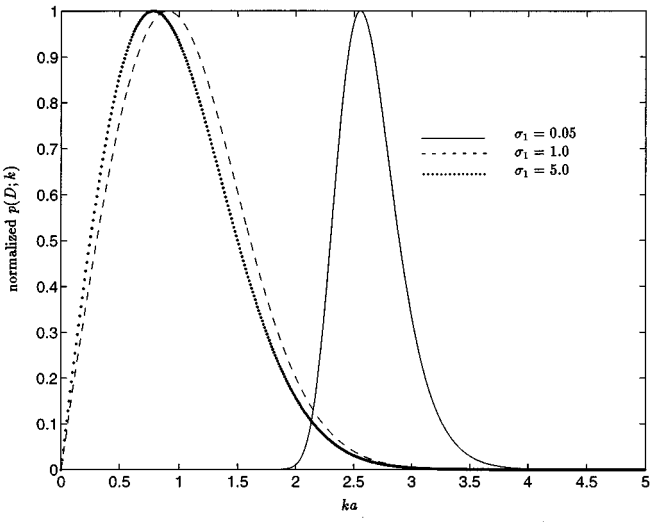

FIG. 5. The normalized pdf of D at frequency k for three values of $\sigma_1(k)$.

IV. A PROBABILITY DENSITY FUNCTION

The error analyses of the previous sections provide information about the best-possible precision and the expected precision in an ideal experiment. The probability density function for $\hat{D}$ offers additional clues that could help us adapt the experimental design in a manner that minimizes error under more general measurement conditions.

The pdf of the echo signal from random scattering media is well known.[18,24] As with the in-phase and quadrature components of the echo signal $x[i]$, the joint pdf of the real and imaginary parts of the complex Fourier amplitude $X(k)=X_r+iX_i$ are completely specified by

$$p(X_r,X_i)=\frac{1}{2\pi\sigma_x^2}\exp\left\{-\frac{X_r^2+X_i^2}{2\sigma_x^2}\right\}. \tag{28}$$

Furthermore, the pdf of the echo intensity $|X(k)|^2$ is

$$p(|X(k)|^2)=\frac{1}{2\sigma_x^2}\exp\left\{-\frac{|X(k)|^2}{2\sigma_x^2}\right\}. \tag{29}$$

Combining Eqs. (14), (15), (29), and using the general transformation property of density functions,

$$p(u)=p(v)\left|\frac{du}{dv}\right|^{-1}, \tag{30}$$

the pdf of the form factor at frequency k may be expressed as

$$p(F;k)=\frac{G_1(k)}{2\sigma_x^2}\exp\left\{-\frac{G_1(k)F(k)}{2\sigma_x^2}\right\},\quad F\geqslant 0, \tag{31}$$

where $G_1(k)\equiv c_1N\Delta t k^4|G(k)|^2$. The mean form factor value at frequency k is $E\{F\}=2\sigma_x^2/G_1(k)$ and the variance is $E\{(F-E\{F\})^2\}=4\sigma_x^4/G_1^2(k)$, so that the ratio $(E\{F\})^2/E\{(F-E\{F\})^2\}=1$, which is the same as that for the echo intensity.[18]

Applying the transformation property of Eq. (30) a second time yields $p(D;k)$. To compute the derivative, we first invert Eq. (8b)

$$D(F)=\sqrt{\frac{d_1^2}{2k^2}}\left\{\ln\left(\frac{1}{F}\right)\right\}^{1/2}, \tag{32}$$

and then find

$$\frac{dD(F)}{dF}=-\sqrt{\frac{d_1^2}{2k^2}}\frac{1}{2F}\left\{\ln\left(\frac{1}{F}\right)\right\}^{-1/2}$$
$$=-\frac{d_1^2}{4k^2}\frac{1}{D}\exp\left\{\frac{2k^2D^2}{d_1^2}\right\}. \tag{33}$$

The final form of Eq. (33) is found using the relation $F=\exp\{-2k^2D^2/d_1^2\}$. From Eqs. (30)–(33), the pdf of the scatterer size D at frequency k is given by

$$p(D;k)=\frac{2k^2D}{d_1^2\sigma_1^2(k)}\exp\left[-\left\{\frac{2k^2D^2}{d_1^2}+\frac{1}{2\sigma_1^2(k)}\right.\right.$$
$$\left.\left.\times\exp\left(-\frac{2k^2D^2}{d_1^2}\right)\right\}\right]\quad D\geqslant 0, \tag{34}$$

where $\sigma_1^2(k)=\sigma_x^2/G_1(k)$. From plots of Eq. (34) in Fig. 5 as a function of $ka=kD/2$, we can obtain much insight into the estimation process once we interpret the meaning of $\sigma_1(k)$.

Wagner *et al.*[18] interpreted the quantity σ_x^2 from the density functions in Eqs. (28) and (29) as the intensity backscattered from a random medium. Using Eq. (8) and the interpretation of σ_x^2 as the backscattered intensity, it can be shown that $\sigma_1^2(k)\propto F(k,D)/|G(k)|^2$, which is the ratio of the tissue spectral density to pulse spectral density at frequency k. When σ_1 is large, the tissue spectrum is broadbanded compared to the pulse spectrum, and Eq. (34) reduces to a Rayleigh pdf:

$$p(D;k)\approx\frac{2k^2D}{d_1^2\sigma_1^2(k)}\exp\left(-\frac{2k^2D^2}{d_1^2}\right)\quad D\geqslant 0. \tag{35}$$

Curves for $\sigma_1>5$ were indistinguishable from the curve for $\sigma_1=5$ shown in Fig. 5. However, when $\sigma_1\approx 1$, the pulse spectrum and tissue spectrum are comparable. Further reductions in σ_1 occur when the pulse length is smaller than the scatterer, which can only happen when $ka>1$. When that occurs,

Eq. (34) is no longer valid because the echo signal, on which Eq. (34) is based, is not well represented by the circular Gaussian pdf of Eq. (28). Rather, expressions for $p(D;k)$ must be derived from non-Gaussian probability models[25,26] when the number of scatterers per resolution cell volume is small. This limitation on the range of validity of this analysis also explains the apparent inconsistency in Eq. (31). While the Rayleigh distribution function given in Eq. (31) extends to infinity, we know that the acoustic form factor is less than one by definition. However, $p(F;k)$ will be nonzero for $F>1$ only when σ_1 is small; therefore, such an inconsistency occurs only outside the domain of validity of the analysis.

Roughly speaking, σ_1 may be interpreted as the number of scatterers per resolution cell volume. When $\sigma_1 \geqslant 5$, $p(D;k)$ is nearly equal to the Rayleigh pdf of Eq. (35). When $1<\sigma_1<5$, then Eq. (35) is a reasonable approximation. However, when $\sigma_1<1$, the scattering medium is sparsely populated by scatterers, and therefore a new pdf of the echo signal must be specified.

In random media that produce echo signals described by Eq. (28), $p(D;k)$ is given by Eq. (35) and by the dotted curve in Fig. 5. It is reasonable to design experiments in which the interrogating frequencies are adjusted depending on the average scatterer size to produce the most likely value of D, which also corresponds to the peak of the dotted curve in Fig. 5. The position of the maximum value of $p(D;k)$ is easily calculated by differentiating Eq. (35) with respect to D and setting the result to zero: $1-4k^2D^2/d_1^2=0$. This shows that $ka=0.8$ is most likely, and confirms our observations based on phantom experiments.[14]

Note that the results of Secs. III and IV can be related since $\operatorname{var}\hat{D}=\int(\hat{D}-D)^2p(D)dD$, where $p(D)=\int p(D;k)dk$.

V. DISCUSSION

It is obvious from Fig. 3 that the scatterer size estimator of Eq. (20) is *not efficient* in the sense that $(\operatorname{var}\hat{D})^{1/2}$ is many times ϵ_D. This finding is not unexpected considering that the efficiency of an estimator is reduced when the data and the estimate are related through a nonlinear transformation,[17] as in Eq. (32). The ratio $(\operatorname{var}\hat{D}/\epsilon_D^2)^{1/2}$ is six for the 200% analysis bandwidth used to generate the data in Fig. 3. However, that ratio increases as the bandwidth is reduced, e.g., the ratio is 12 for a 67% bandwidth.

The $\operatorname{var}\hat{D}$ can be reduced in two ways. First, if the input SNR is large, then a wideband transducer can be used to increase the number of points in the analysis bandwidth. As shown in Fig. 4 and Eq. (27), a larger bandwidth increases the number of independent samples used in the estimation of $\hat{D}$, and $\operatorname{var}\hat{D}\sim k^{-4}$. If SNR is small, then $\operatorname{var}\hat{D}$ can be reduced by averaging P estimates from P adjacent but uncorrelated echo waveforms: $D=1/P\Sigma_{i=1}^{P}\hat{D}_i$. The relative variance, $\operatorname{var}D/\operatorname{var}\hat{D}=1/P$, is reduced at the expense of spatial resolution. Note that because of the nonlinear transformation, obtaining a single scatterer size estimate from an average form factor is not equivalent to averaging $\hat{D}$ obtained from individual waveforms. While the benefit of averaging estimates is task dependent, it is always helpful to increase the analysis bandwidth as much as the noise will allow. However, increasing the frequency and the bandwidth works only if $k_0a\approx 1$ for the reasons detailed at the end of Sec. IV, which emphasize the need for some prior information about the medium under investigation.

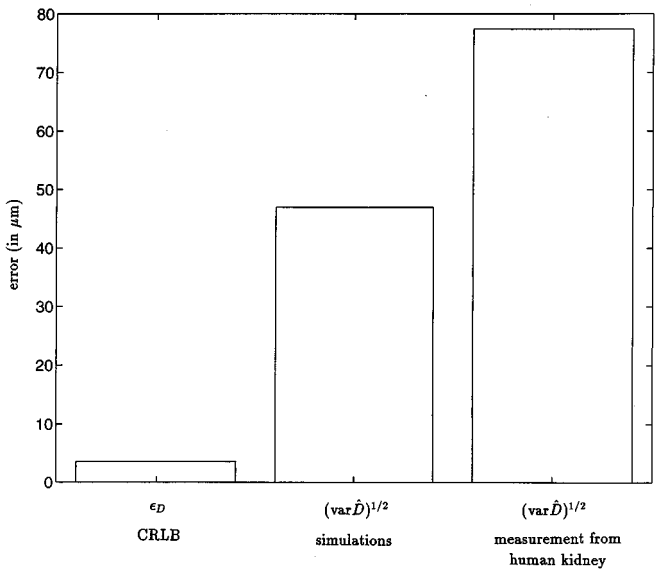

FIG. 6. Comparison of measured and predicted scatterer size errors. All errors are for normal human renal cortex at 3 MHz, and a single 256 point waveform is used for estimation.

Figure 4 shows that Eq. (27) accurately predicts $\operatorname{var}\hat{D}$ if the analysis bandwidth exceeds 70%–80% of the transducer center frequency. At smaller bandwidths the approximation involving the Taylor series expansion of $\hat{F}$ breaks down and Eq. (27) underestimates the error. In our experience studying renal tissue,[1] the -20-dB bandwidth often exceeds 70% of the center frequency, so that Eq. (27) is a good approximation of the variance.

If the PSD is estimated by a technique other than the periodogram, the variance given by Eq. (27) is still valid if the appropriate expression for the variance of the PSD is used. The procedure for estimating the echo-signal power spectral density (PSD) affects $\operatorname{var}\hat{D}$ through the variance of the form factor. Therefore, additional independent sources of measurement variance $\operatorname{var}_{\text{meas}}$ can be incorporated into the model by substituting $\operatorname{var}\hat{F}(k_i)+\operatorname{var}_{\text{meas}}$ in place of $\operatorname{var}\hat{F}(k_i)$ in Eq. (22).

Finally, we place the results of this paper in the context of *in vivo* scatterer size measurements made from the renal cortex of normal adult human volunteers.[27] Data for volunteers with similar weights and body compositions was considered to minimize interpatient biological variability. The average scatterer size in 50 subjects using a single waveform for each estimate was found to be 210 ± 7.74 μm. A 3-MHz transducer ($k_0a=1.28$) provided a 67% analysis bandwidth (2–4 MHz), and the waveforms were 10.2 μs in duration ($N=256$ pts). The measured errors in $\hat{D}$, those predicted using the CRLB expression of Eq. (3) analogous to an infinite bandwidth, and using Eq. (27) with a 67% bandwidth for the same conditions are displayed in Fig. 6. For all errors shown in the figure, *a single 256-point waveform* was used to obtain the estimate. Errors for the *in vivo* results include

measurement error as well as biological uncertainty. The *in vivo* data were reduced to a single waveform estimate by multiplying the standard deviation by ten (two kidneys for each of the 50 patients) to account for the $1/N$ dependence of the variance. Comparing results of Fig. 6, we conclude that the estimation uncertainty is at least as large as that caused by biological variability.

VI. CONCLUSIONS

It is shown that Eq. (27) may be used to accurately predict var $\hat{D}$ when the analysis bandwidth exceeds 80% of the center frequency. The scatterer size estimator of Eq. (20) does not reach the CRLB because of the nonlinear relationship between the echo data and D. Furthermore, the discrepancy between the achievable error and the lower bound is at least as large as the biological variability, suggesting that a more efficient estimator might be obtained.

The lowest achievable error in scatterer size is found using the largest analysis bandwidth (determined by the SNR of the echo signal) and a center frequency that satisfies the relation $k_0 a \simeq 0.8$. These analytical results are consistent with experimental findings reported earlier.[14]

ACKNOWLEDGMENTS

This work was supported by the National Institutes of Health under Grant No. R01 DK 43007 and by the Clinical Radiology Foundation at KUMC.

[1] M. F. Insana, J. G. Wood, and T. J. Hall, ''Identifying acoustic scattering sources in normal renal parenchyma in vivo by varying arterial and ureteral pressures,'' Ultrasound Med. Biol. **18**, 587–599 (1992).

[2] M. F. Insana, J. G. Wood, T. J. Hall, G. G. Cox, and L. A. Harrison, ''Effects of endothelin-1 on renal microvasculature measured using quantitative ultrasound,'' Ultrasound Med. Biol. **21**, 1143–1151 (1995).

[3] S. Ito, L. A. Juncos, N. Nyshiro, C. S. Johnson, and O. A. Carretero, ''Endothelium-derived relaxing factor modulates endothelin action in afferent arterioles,'' Hypertension **17**, 1052–1056 (1991).

[4] P. M. Morse and K. U. Ingard, *Theoretical Acoustics* (McGraw-Hill, New York, 1968), Section 8.2.

[5] A. Ishimaru, *Wave Propagation and Scattering in Random Media* (Academic, New York, 1978), Vol. 1, Chap. 5.

[6] J. A. Campbell and R. C. Waag, ''Ultrasonic scattering properties of three random media with implications for tissue characterization,'' J. Acoust. Soc. Am. **75**, 1879–1886 (1984).

[7] M. F. Insana, R. F. Wagner, D. G. Brown, and T. J. Hall, ''Describing small-scale structure in random media using pulse-echo ultrasound,'' J. Acoust. Soc. Am. **87**, 179–192 (1990).

[8] F. L. Lizzi, M. Ostromogilsky, E. J. Feleppa, M. C. Rorke, and M. M. Yaremko, ''Relationship of ultrasonic spectral parameters to features of tissue microstructure,'' IEEE Trans. Ultrason. Ferroelect. Freq. Control **34**, 319–329 (1987).

[9] J. A. Campbell and R. C. Waag, ''Normalization of ultrasonic scattering measurements to obtain average differential scattering cross sections for tissues,'' J. Acoust. Soc. Am. **74**, 393–399 (1983).

[10] M. F. Insana, T. J. Hall, and L. T. Cook, ''Backscatter coefficient estimation using array transducers,'' IEEE Trans. Ultrason. Ferroelect. Freq. Control **41**, 714–723 (1994).

[11] E. L. Madsen, M. F. Insana, and J. A. Zagzebski, ''Method of data reduction for accurate determination of acoustic backscatter coefficients,'' J. Acoust. Soc. Am. **76**, 913–923 (1984).

[12] J. E. Perez, J. G. Miller, M. R. Holland, S. A. Wickline, A. D. Waggoner, B. Barzilai, and B. E. Sobel, ''Ultrasonic tissue characterization: integrated backscatter imaging for detecting myocardial structural properties and on-line quantitation of cardiac function,'' Am. J. Card. Imag. **8**, 106–112 (1994).

[13] M. F. Insana, ''Modeling acoustic backscatter from kidney microstructure using an anisotropic correlation function,'' J. Acoust. Soc. Am. **97**, 649–655 (1995).

[14] M. F. Insana and T. J. Hall, ''Parametric ultrasound imaging from backscatter coefficient measurements: image formation and interpretation,'' Ultrason. Imag. **12**, 245–267 (1990).

[15] M. F. Insana and D. G. Brown, ''Acoustic scattering theory applied to soft biological tissues,'' in *Ultrasonic Scattering in Biological Tissues*, edited by K. K. Shung and G. A. Thieme (CRC, Boca Raton, FL, 1993), pp. 75–124.

[16] Straight brackets indicate temporal sampling as in $s[i]$ and subscripted angle brackets indicate spatial sampling as in $r_{\langle m \rangle}$.

[17] S. M. Kay, *Fundamentals of Statistical Signal Processing: Estimation Theory* (Prentice-Hall, Englewood Cliffs, NJ, 1993).

[18] R. F. Wagner, S. W. Smith, J. M. Sandrik, and H. Lopez, ''Statistics of speckle in ultrasound B-scans,'' IEEE Trans. Sonics Ultrason. **30**, 156–163 (1983).

[19] D-L. Liu, K. Ikeda, and M. Saito, ''On the method-independent lower bound (MILB) to the variance of attenuation estimation in random reflection,'' IEEE Trans. Med. Imag. **9**, 43–48 (1990).

[20] For $g[i]$ to be spatially invariant, the signals must be compensated for ultrasonic attenuation or the attenuation must be small over the N samples so that $g[i]$ does not vary significantly with depth. For example, at 3 MHz, with an attenuation coefficient of 0.4 dB cm^{-1} MHz^{-1}, and over a 4 mm depth ($N=128$ for a 2.5×10^7 samples per second rate) the amplitude loss is only 10%.

[21] Note that $D/\text{FWHM} = (12\sqrt{2\pi})^{1/3} d/2\sqrt{2\ln 2}\sigma_g \simeq 1.32 d/\sigma_g$.

[22] S. L. Marple, *Digital Spectral Analysis With Applications* (Prentice-Hall, Englewood Cliffs, NJ, 1987).

[23] P. R. Bevington, *Data Reduction and Error Analysis for the Physical Sciences* (McGraw-Hill, New York, 1969).

[24] R. F. Wagner, M. F. Insana, and D. G. Brown, ''Statistical properties of radio-frequency and envelope detected signals with applications to medical ultrasound,'' J. Opt. Soc. Am. A **4**, 910–922 (1987).

[25] P. N. Pusey, D. W. Schaefer, and D. E. Koppel, ''Single-interval statistics of light scattered by identical independent scatterers,'' J. Phys. A: Math, Nucl. Gen. **7**, 530–540 (1974).

[26] J. W. Strutt (Lord Rayleigh), ''On the problem of random vibrations, and of random flights in one, two, or three dimensions,'' Philos. Mag. **37**, 321–347 (1919).

[27] T. J. Hall, M. F. Insana, G. G. Cox, and L. A. Harrison, ''Ultrasonic measurement of glomerular diameters in normal adult humans,'' Ultrasound Med. Biol., Fig. 9 (under review).